

An investigation of the influence of supraglacial debris on glacier hydrology

1

2 **C. L. Fyffe¹, B. W. Brock², M. P. Kirkbride³, D.W.F. Mair⁴, N. S. Arnold⁵,**
3 **C. Smiraglia⁶, G. Diolaiuti⁶ and F. Diotri⁷**

4 [1] Institute of Science and the Environment, University of Worcester, Worcester, United
5 Kingdom

6 [2] Department of Geography, Northumbria University, Newcastle, United Kingdom

7 [3] School of the Environment, University of Dundee, Dundee, United Kingdom

8 [4] School of Environmental Sciences, University of Liverpool, Liverpool, United Kingdom

9 [5] Department of Geography, University of Cambridge, Cambridge, United Kingdom

10 [6] Department of Earth Sciences 'Ardito Desio', University of Milan, Milan, Italy

11 [7] Agenzia Regionale per la Protezione dell'Ambiente della Valle d'Aosta, Aosta, Italy

12 Correspondence to: C. L. Fyffe (catrionalfyffe@live.com)

13 **Abstract**

14 The influence of supraglacial debris on the rate and spatial distribution of glacier surface melt
15 is well established, but its potential impact on the structure and evolution of the drainage
16 system of extensively debris-covered glaciers has not been previously investigated. Forty-
17 eight dye injections were conducted on Miage Glacier, Italian Alps, throughout the 2010 and
18 2011 ablation seasons. An efficient conduit system emanates from moulins in the ~~mid-part of~~
19 ~~the glacier~~ **central ablation area**, which are downstream of a high-melt area of dirty ice and
20 patchy debris. High melt rates and runoff concentration by intermoraine troughs encourages
21 the early-season development of a channelized system downstream of this area. Conversely,
22 the drainage system beneath the continuously debris-covered lower ablation area is generally
23 inefficient, with multi-peaked traces suggesting a distributed network, which likely feeds into
24 the conduit system fed by the upglacier moulins. Drainage efficiency from the debris-covered
25 area increased over the season but trace ~~flow velocity~~ **transit velocity** remained lower than
26 from the upper glacier moulins. Low and less-peaked melt inputs combined with the

27 | hummocky topography of the debris-covered area inhibits the formation of an efficient
28 drainage network. These findings are relevant to regions with extensive glacial debris cover
29 and where debris cover is expanding.

30 **1 Introduction**

31 Debris-covered glaciers are prevalent in mountainous regions such as the Pamirs and
32 Himalaya (Scherler et al., 2011; Bolch et al., 2012), Caucasus Mountains, Russia (Stokes et
33 al., 2007), and the Western Alps (Deline et al., 2012) and the extent and thickness of debris-
34 cover on glaciers is increasing in many regions (Bolch et al., 2008; Bhambri et al., 2011;
35 Lambrecht et al., 2011; Kirkbride and Deline 2013). Glacier-runoff is important for
36 downstream water resources, especially during dry seasons (Xu et al., 2009; Maurya et al.,
37 2011). The ablation of ice has a non-linear relationship to the thickness of the overlying
38 debris, with the exact relationship determined by the debris thermal and radiative properties.
39 The relationship between ablation and debris thickness has been derived for several different
40 glaciers and surface covers (e.g. Østrem (1959), Mattson et al. (1993) and Kirkbride and
41 Dugmore (2003)). The dominant effect is a reduction in the melt rate compared with that of
42 bare ice where debris is continuous and more than a few centimetres thick (Brock et al.,
43 2010), with recent hourly energy balance modelling suggesting the debris causes attenuation
44 of the diurnal melt signal (Fyffe et al., 2014).

45 On debris-free temperate glaciers, dye-tracing studies have demonstrated that the seasonal
46 evolution of the hydrological system, characterised by increasing efficiency over time, is
47 closely linked to the increase in volume and daily amplitude of surface meltwater inputs
48 associated with the upglacier retreat of the seasonal snowline (Nienow et al., 1998; Willis et
49 al., 2002; Campbell et al., 2006). Understanding the nature and evolution of the glacial
50 drainage system is important because it controls how meltwater inputs impact glacial
51 dynamics (e.g. Mair et al., 2002), with the glacial dynamic response affecting erosion rates
52 (Hallet et al., 1996). Any overall impact on glacier dynamics will also have an influence on
53 the glacier's mass balance. If the debris influences the glacier hydrological system then this
54 could impact on the timing of the transfer of water through the system, influencing the
55 proglacial runoff signal. However, only Hasnain et al. (2001) have carried out dye tracing on
56 a debris-covered glacier, focussing on the autumn close-down rather than the spring evolution
57 of the hydrological system, and not dealing explicitly with the influence of debris cover.
58 Direct investigation of englacial conduit systems within debris-covered glaciers (e.g. Gulley

59 and Benn, 2007) have not yet revealed the morphology of inaccessible regions, or gauged the
60 efficiency of the entire system. Considering the strong influence debris has on surface
61 ablation rates (Nicholson and Benn, 2006; Lejeune et al., 2013; Fyffe et al., 2014) extensive
62 debris cover can be expected to influence the morphology and evolution of a glacier's
63 hydrological system, but the nature and extent of this impact is not currently known. Based
64 on field investigations at an alpine debris-covered glacier, this study therefore has two aims:

- 65 1. To investigate the impact of debris on the supraglacial topography, and, combined
66 with knowledge of the debris' influence on melt rates and measurements of
67 supraglacial flow, assess the likely influence of the debris cover on the amplitude and
68 magnitude of surface meltwater inputs.~~To understand the influence of debris cover on~~
69 ~~the daily amplitude and magnitude of surface meltwater input to the glacial drainage~~
70 ~~system.~~
- 71 2. To determine the morphology and seasonal evolution of the englacial and subglacial
72 hydrological system and its relationship to the spatial distribution of supraglacial
73 debris cover.

74 Our investigation is guided by two overarching hypotheses: ~~F~~are first, that continuous
75 debris cover over the lower glacier inhibits the development of an efficient channelized
76 drainage system, both through suppression of surface melt beneath thick debris and the
77 formation of hummocky surface topography which impedes drainage capture and leads to
78 low magnitude and dispersed meltwater inputs to the glacier; and second, that above the
79 upper limit of continuous debris cover, the development of an efficient channelized
80 drainage system is promoted both by the enhancement of melt beneath thin and patchy
81 debris and the formation of ridge-valley topography which enhances surface drainage
82 capture and concentrates rapid surface melt into high magnitude moulin inputs. These
83 hypotheses are investigated by the measurement of supraglacial flow and 48 dye
84 injections into 16 surface streams over 2 ablation seasons. These measurements are
85 interpreted to explain the drainage system configuration emanating from the continuously
86 and partly debris-covered parts of the glacier, their interaction and evolution over the
87 course of the ablation season.

88 2 Study Site

89 Miage Glacier is situated in the Western Italian Alps (Fig. 1). It originates from four main
90 tributaries, the Mont Blanc, Dome, Bionassay and Tête Carrée Glaciers, which form steep

91 icefalls prior to joining the main tongue. As the main tongue enters Val Veny it bends
92 eastwards before splitting into the large northern and southern lobes and smaller central lobe.
93 The glacier area is 10.5 km² over an elevation range of 1740 to 4640 m a.s.l.. The lower 5 km
94 of the glacier is completely covered by debris which averages 0.25 m in thickness (Foster et
95 al., 2012), except for isolated debris-free ice cliffs (Reid and Brock, 2014). The debris
96 increases in thickness with distance down glacier so that over most of the lower tongue it is
97 thicker than the ‘critical thickness’ (see Kirkbride and Dugmore, 2003), resulting in reduced
98 ablation compared to bare ice. At higher elevations (above c. 2500 m a.s.l.) the debris is
99 confined to medial and lateral moraines with the intervening ice having a patchy covering of
100 dust to boulder sized sediment (hereafter ‘dirty ice’). The debris originates predominantly
101 from rockfalls and mixed snow and rock avalanches from the steep valley sides (Deline,
102 2009). Diolaiuti et al. (2009) found that the debris cover, and its influence on ablation,
103 strongly influenced changes in the glacier’s volume over time. A distributed surface energy-
104 balance melt model for the glacier was recently developed by the authors and used to explore
105 patterns and rates of surface melting (Fyffe et al., 2014).

106 **3 Methods**

107 **3.1 Runoff**

108 **3.1.1 Proglacial runoff**

109 Field data were collected at Miage Glacier over two ablation seasons, from 5 June
110 ~~05/06/2010~~ to 13 September ~~3/09/2010~~, and from 04 June ~~/06/2011~~ to 16 September
111 ~~/09/2011~~.

112 The main outflow stream from the glacier exits the northern lobe, while very little drainage
113 exits the southern lobe. Discharge was monitored at a gauging station directly downstream of
114 the northern portal (Fig. 1). Stage was measured using a pressure transducer mounted in a
115 well attached to a large, stable boulder (see Table 1 for details). The Onset HOBO pressure
116 data were compensated using air pressure data from Mont de la Saxe, 7.6 km from the
117 gauging station. A high flow event in June 2011 caused damage to the well, resulting in lost
118 data between 18 June ~~/06/2011~~ and 3 August ~~03/08/2011~~ and the repositioning of the well.

119 Other data voids are 27 to 28 August ~~/08/2010 to 28/08/2010~~ and 04 to 8 September
120 ~~2010/09/2010 to 08/09/2010~~. All recorded stages were adjusted to the datum of the June 2010

121 stilling well so that a single stage-discharge rating could be applied to the entire record. The
122 stage-discharge rating was derived from discharges calculated from dye dilution gauging
123 using rhodamine WT. In total 16 dye dilution gaugings performed in both 2010 and 2011
124 provided a two-part rating curve which has a standard error of the estimate of $0.76 \text{ m}^3 \text{ s}^{-1}$,
125 which gave a percentage error of 14.6% using the average daily discharge in 2010 of 5.37 m^3
126 s^{-1} . The use of a single rating curve for the whole period was justified by the correspondence
127 of gaugings from different field visits.

128 **3.1.2 Supraglacial stream measurements**

129 Prior to conducting a dye trace, the discharge and velocity of the chosen supraglacial stream
130 (Q_s and u_s , respectively) were measured in 2011. Either the velocity-area method or salt
131 dilution gauging was used to measure supraglacial stream discharge. Dilution gauging was
132 preferred, but this was not always possible. The cross sectional area was calculated by
133 multiplying the stream width by the depth, measured on average at 9 points across the
134 channel. Surface velocity was measured by timing the passage of floats using floats, which are
135 likely to overestimate mean depth-averaged velocity (Dingman, 2002). Floats usually
136 followed the stream thalweg and so travelled faster than the width and depth-averaged flow.
137 The salt dilution gauging was performed using a portable conductivity probe (Table 1).

138 The dilution gauging velocity is the distance between injection and detection points divided
139 by the time between injection and peak of the concentration curve. This gives the average
140 water velocity, a preferable measure of velocity than the float method. Therefore, discharges
141 measured using the velocity-area method were adjusted using the ratio of dilution to float
142 velocity found from simultaneous measurements.

143 **3.2 Delimiting supraglacial catchments and routing**

144 Supraglacial streams and their catchments were defined by applying Arnold (2010)'s lake and
145 catchment identification algorithm (LCIA) to a digital elevation model (DEM). The algorithm
146 calculates surface slope and direction of steepest descent (flow direction) for each cell. Sinks
147 (potential lakes) are defined as cells with no lower neighbours, with the algorithm using the
148 flow direction matrix to find the upstream cells that feed to that sink. The catchment outlet is
149 determined as the lowest cell on the catchment boundary, with each cell lower than this
150 within the catchment flooded with water to identify lakes. The algorithm also determines the
151 flow pathways between each catchment allowing the entire supraglacial stream and lake
152 network to be defined. This supraglacial algorithm is favoured over most others because it

153 does not rely on the artificial filling of sinks before calculating the flow routing. Arnold
154 (2010) provides detailed model methods. The DEM was derived from airborne LiDAR
155 surveys in 2008 (provided by Regione Autonoma Valle d'Aosta, VDA DEM hereafter) and
156 has a spatial resolution of 2 m and a vertical accuracy of < 0.5 m. The VDA DEM was
157 resampled to a 4 m cell size and was clipped to the glacier catchment boundary which follows
158 the mountain ridge surrounding the glacier and the moraine crests outside of the glacial
159 trough.

160 **3.3 Ice thickness**

161 Ice thickness data was required to calculate the conduit closure rates (see Appendix A). The
162 ice thickness is calculated as the difference between the surface and bed elevation. The VDA
163 DEM was used to give the surface topography. A map of the bed topography in Deline
164 (2002) (based on Carabelli (1961), Casati (1998) and Lesca (1974)), was scanned,
165 georeferenced, digitised and interpolated into a raster with a 25 m cell size. Unfortunately,
166 the resolution of the map contours was low and the fit of the map to the glacier outline was
167 poor due to a lack of clear control points. Resulting conduit closure rates should therefore be
168 treated with caution.

169 **3.4 Meteorological stations**

170 Three meteorological stations were located on the glacier. The lower and upper weather
171 stations (LWS and UWS hereafter) were full energy-balance stations situated on continuous
172 debris cover, with the ice weather station (IWS) measuring only air temperature on an area of
173 dirty ice (Fig. 1). Details of the instruments installed on LWS, UWS and IWS are given in
174 Brock et al. (2010) and Fyffe et al. (2014).

175 **3.5 Dye tracing**

176 In total 48 dye injections were conducted into 16 surface streams. All dye traces were carried
177 out using 21% rhodamine WT liquid dye. Between 40 and 280 ml of dye was used per
178 injection. To allow comparison of breakthrough curves from the same streams repeat traces
179 were conducted at similar times of day, particularly for upglacier streams. The injection times
180 range for streams traced on multiple occasions (for successful traces) are 14:27-16:50 (S3),
181 13:00-17:10 (S5/S5b), 16:31-19:02 (S7), 15:15-16:22 (S12/S12b), 12:08-15:12 (S14/S14b)
182 and 13:18-15:29 (S15). The dye trace was detected at the gauging station using a fluorometer
183 (see Table 1) recorded by a Campbell logger (CR500, until 14 ~~June /06/20~~11 when it was

184 replaced with a CR10X) at either 5 or 1 minute intervals. Each fluorometer was calibrated in
185 the field ~~with~~for each ~~batch of dye~~dye lot.

186 Although it was intended to use injection points which led directly into a moulin, this often
187 wasn't possible especially on the lower glacier where streams could become hidden by
188 debris. The moulins were not located for the S1, S2 and S6 streams; for S3 and S4 the stream
189 did apparently disappear into a moulin a few metres from the injection point but this was
190 hidden by large boulders; S7 did become englacial a short distance from the injection site but
191 through the 'cut and closure' mechanism rather than a moulin; whereas the S8 injection was
192 directly into an englacial conduit. The injection point into S5 was into a stream 446 m
193 upstream of the moulin and so the trace transit velocity (μ) was adjusted to account for the
194 time spent in the supraglacial stream, using the measured supraglacial stream velocity (u_s) at
195 the time of the test (2011 only). Henceforth, only adjusted μ is given, especially where debris
196 cover was thick. Streams often flow beneath the debris, making it difficult to inject dye. In
197 some cases, difficulty in accessing moulins due to ice cliffs meant an injection point was used
198 further upstream.

Formatted: Font: Italic

Formatted: Font: Italic

Formatted: Font: Italic, Subscript

Formatted: Font: Italic

199 During 2011 the execution of repeat injections at individual points was emphasised. Five
200 injection points were chosen, two on the lower glacier debris zone (S5 and S7), and three on
201 the upper glacier debris zone (S12, S14 and S15) (see Fig. 1). The three upper points were
202 intended to be spread equally along the glacier, but following an extensive search the only
203 moulins found were all in a relatively small area.

204 Although theThe parameters calculated for each dye-breakthrough curve are given in Table 2,
205 further detail of the calculation of some these parameters is warranted. The dispersion
206 coefficient ($D, m^2 s^{-1}$) is calculated from:

$$207 \quad D = \frac{d^2(t-t_i)^2}{4t^2t_i \ln \left[2 \left(\frac{t}{t_i} \right)^{\frac{1}{2}} \right]} \quad (1)$$

Formatted: Font: Italic

Formatted: Font: Not Italic

Formatted: Font: Not Italic, Superscript

Formatted: Font: Not Italic

Formatted: Font: Not Italic, Superscript

208 (Seaberg et al., 1988, p222), with t_i the time from injection to half of the dye concentration
209 peak on the rising limb and again for the falling limb, with t as used in this equation (time
210 between injection and dye concentration peak), not measured but found iteratively by
211 determining the value which minimises the difference between the two variants of equation 1.
212 The calculated value of t is then used to compute D with either value of t_i . The volume of

Formatted: Font: Italic

Formatted: Font: Italic, Subscript

Formatted: Font: Italic

Formatted: Font: Italic

Formatted: Font: Italic

Formatted: Font: Italic

Formatted: Font: Italic

Formatted: Font: Italic, Subscript

213 dye recovered (V_r , ml) is calculated from equation 2, which was derived from the equation to
214 calculate discharge from dilution gauging given by Kilpatrick and Cobb (1985, p6):

$$215 \quad V_r = \frac{S^{-1} \left(\frac{1}{1.649 \times 10^{-8}} (Q_p A_c) \right)}{c_{di}} \quad (2)$$

216 where S is the specific gravity of the dye used (1.15 for rhodamine WT), Q_p ($m^3 s^{-1}$) is the
217 average proglacial discharge from the time of injection until the time of the peak of the dye
218 return curve and c_{di} (ppb) is the concentration of the dye prior to injection. A_c (ppb minute) is
219 the area under the dye breakthrough curve, calculated by summing all of the dye
220 concentration values composing the breakthrough curve and multiplying this by the logging
221 interval between measurements in minutes. The injection point into S5 was into a stream 446
222 m upstream of the moulin and so the trace flow velocity (u) was adjusted to account for the
223 time spent in the supraglacial stream, using the measured supraglacial stream velocity (u_s) at
224 the time of the test (2011 only). Henceforth, only adjusted u is given.

225 4 Results

226 4.1 Meteorological and Snow Cover Conditions

227 An overview of the air temperature, discharge and precipitation in both years is given in Fig.
228 2. On average, air temperatures between 5 June and 12 September at LWS were similar in
229 2010 and 2011 (10.9°C and 10.8°C, respectively). June was relatively cool in both years;
230 although a rise in air temperature along with heavy rainfall resulted in a significant increase
231 in discharge on 18 ~~June~~ June 2011. In early June 2010 snow cover was continuous above 2290
232 m a.s.l. (close to S9). In contrast, the continuously debris-covered zone was mainly snow free
233 in early June 2011, with continuous snow cover only above 2400 m a.s.l., due to prolonged
234 high temperatures in May (Fig. 2b). Clean ice was exposed in places on the main tongue,
235 above the Dome Glacier confluence. July 2010 was warmer than July 2011 (mean LWS air
236 temperatures were 13.1°C and 9.4°C, respectively) whereas August and early September
237 were cooler in 2010 than in 2011, (mean LWS air temperature 10.5°C and 12.6°C in August,
238 and 9.1°C and 11.5°C in early September, respectively).

239 4.2 Supraglacial hydrology

240 The values of mean Q_s and u_s for each of the 2011 streams is given in Table 3, with values
241 for each injection time are given in Table 4. S14 (the main stream draining the western side of

Formatted: Font: Italic

Formatted: Font: Italic, Subscript

Formatted: Font: Not Italic

Formatted: Font: Italic

Formatted: Font: Italic

Formatted: Font: Italic, Subscript

Formatted: Superscript

Formatted: Superscript

Formatted: Font: Italic

Formatted: Font: Italic, Subscript

Formatted: Font: Italic

Formatted: Font: Italic, Subscript

Formatted

242 the upper glacier, Fig. 3c) and S12 (the main stream draining the eastern side of the upper
243 glacier, Fig. 3b) had the highest Q_s and u_s of those measured. The Q_s range was 0.378-0.888
244 m^3s^{-1} for S14 and 0.025-0.341 m^3s^{-1} for S12 and the u_s range was 0.92-2.16 ms^{-1} for S14 and
245 0.43-0.50 ms^{-1} for S12. These streams had relatively large catchments bounded laterally by
246 the central and lateral moraine crests (Figs. 4 and 5). Supraglacial streams were difficult to
247 find on the continuously debris-covered zone, and there was a lack of well-defined moulins.
248 Streams cut laterally into the ice, forming ice cliffs from which the debris collapses, hiding
249 the stream beneath the boulders. S5 (the largest stream observed on the lower glacier) and S7
250 both had relatively low Q_s and u_s . The Q_s range was 0.027-0.032 m^3s^{-1} for S5 and 0.006-0.032
251 m^3s^{-1} for S7 and the u_s range was 0.13-0.25 ms^{-1} for S5 and 0.17-0.28 ms^{-1} for S7. Figure 5
252 clearly shows that on the lower glacier catchment sizes are smaller and no longer controlled
253 by the lateral moraines.

254 4.3 Englacial and subglacial hydrology

255 Dye trace parameters for all 2010 and 2011 injections are reported in Tables 3 and 4, with
256 dye return curves shown in Figs. 6, 7 and 8. For ease of reference, injections into S9 and
257 above will be termed upper glacier traces (zone of patchy debris and bare ice), while those
258 into S8 and below will be termed lower glacier traces (continuously debris-covered ice).

259 4.3.1 Spatial Patterns

260 Generally, the water entering the glacier via the main moulins around the upper limit of
261 continuous debris cover travelled quickly to the proglacial stream, with mean u of the upper
262 glacier traces (S10-S15) being 0.56 ms^{-1} . These traces also generally had single-peaked return
263 curves (Figs. 6a and 7d-f) and relatively high percentage dye returns (P_r), confirming that the
264 majority of the water was routed efficiently. Most streams from the lower glacier had low u
265 (the average for all lower glacier injection points was 0.26 ms^{-1}), with the exception of S6 and
266 S8 (Figs. 3a and 6a) which had a faster u of 0.58 ms^{-1} and 0.43 ms^{-1} , respectively. However,
267 generally meltwater produced on the upper glacier could reach the proglacial stream before
268 meltwater produced at the same time on the lower glacier. Return curves from lower glacier
269 traces were generally broader and several displayed multiple peaks (Figs. 6b and 7a-c).

270 A striking result is that average u increases with distance upglacier and is significantly
271 positively correlated with the distance from the gauging station, (p-value = 0.005, Pearson's
272 $r = 0.708$) (Fig. 9a). P_r was also significantly positively correlated with distance from the
273 gauging station (Fig. 9b, p-value = 0.025, Pearson's $r = 0.641$, excluding P_r values greater

Formatted: Font: Italic

Formatted: Font: Italic, Subscript

Formatted: Superscript

Formatted: Superscript

Formatted: Superscript

Formatted: Superscript

Formatted: Font: Italic

Formatted: Font: Italic, Subscript

Formatted: Superscript

Formatted: Superscript

274 than 100%). The average P_r for injection points below and including S10 was always less
275 than 44% with an average of 34%, while for injection points S11 and above the average P_r
276 was at least 50% with an average of 63%.

277 4.3.2 Seasonal evolution

278 *Lower glacier*

279 Lower glacier traces in early June were generally slow (e.g. traces into S1, S3, S5 and S7 had
280 $u < 0.2 \text{ m s}^{-1}$) and often displayed multiple peaks (e.g. S5_06Jun0611 and S7_05Jun0611,
281 Figs. 7b and c). The shape of the S5 dye breakthrough curve changed from ~~sevenix~~ to three
282 more prominent peaks between ~~06 and 12 June /06/2011 and 12/06/2011~~ (Fig. 7b) despite u
283 remaining at 0.07 ms^{-1} . Similarly, there was a change between S7_05Jun0611 and
284 S7_11Jun0611 from a multi-peaked return curve to a curve with one steeply-rising main peak
285 (Fig. 7c).

286 Between June and July 2011 u at S5 increased substantially, the dispersion coefficient (D)
287 and dispersivity (b) decreased markedly and P_r increased, even though the July input
288 discharge was similar to June. The shape of the dye breakthrough curve changed to a steeply
289 rising main peak, with a later secondary peak (Fig. 7b), similar to the trace shape and P_r at the
290 same stage in 2010 (S5_30Jul0710, Fig. 7b). The S3_29Jul0710 trace produced a single ~~leular~~
291 peak, much clearer than its June counterpart, with a faster u and much larger P_r (Fig. 7a).

292 In September the S3_09Sep0910 u was slower than in July but faster than June and had twice
293 the D of the S3_29Jul0710 trace (Fig. 7a and Table 3). The S5_12Sep0911 trace showed the
294 slowest u of the season and was composed of small peaks before and after a broad main peak
295 (Fig. 7b). Misleadingly, D and b values were the lowest of the season because they were
296 calculated from only the main peak. The form of the trace suggests a complex drainage
297 system composed of a small, fast path, a separate slower but larger path, and a third even
298 slower, small path.

299 *Upper glacier*

300 Most upper glacier traces in June (into S10, S12, S13, S14) had $u > 0.4 \text{ m s}^{-1}$, with low D and
301 b , despite the early season stage and extensive snow cover on the upper glacier. Traces
302 tended to give discrete, narrow peaks, although the secondary peak on the S13_11Jun0610
303 trace may suggest temporary water storage in the moulin or a secondary channel (Fig. 8). The

304 | shoulder of the S15_13Jun0611 trace (Fig. 8) might indicate an englacial channel
305 | constriction, past which water was released gradually.

306 | Comparing June and July traces, the S15_28Jul0711 u was much faster than in June (Fig. 7f)
307 | and no longer had a flat top to the trace, causing a reduction in D and b . Conversely, S14 and
308 | S12 u was slower than in June, with larger D and b values (13 times larger for S12, Table 4).
309 | July input discharges into both moulins were larger than in June. S12, S14 and S15 were all
310 | injected again 3 or 4 days later at the start of August. The flow velocities of all three traces
311 | were faster than those in late July along with markedly lower D values (Table 4). The channel
312 | cross-sectional area (A_m) of all three moulins had also increased since late July. Early August
313 | input discharges of S15 and S14 were slightly larger than in July, although for S12 the input
314 | discharge was less than half that measured on 30 July /07/2011. All three breakthrough
315 | curves were of single peaks (Fig. 7d-f).

316 | The September traces into S12, S14 and S15 showed faster u than the June and end of July
317 | traces, but similar, or in the case of S12, slightly slower than their early August traces (Fig.
318 | 7d-f and Table 4). D was also greater than in early August, and in the case of S12 and S14
319 | greater than in June.

320 | **5 Interpretation and discussion**

321 | **5.1 The influence of supraglacial debris on glacial topography and hydrology**

322 | In the region of the glacier between approximately 2300 and 2500 m a.s.l., surface
323 | topography is strongly controlled by contrasting ablation rates between thick moraine-crest
324 | debris, and partly debris-covered ice in the intervening troughs, resulting in longitudinal
325 | ridges and valleys of 30-40 m vertical amplitude (Fig. 4). Ridge-crest ablation is low at
326 | around 0.02 m d^{-1} , compared to 0.05 m d^{-1} in the intermoraine areas, representing the highest
327 | ablation rates on the glacier over an extensive area of thin and partial debris cover
328 | immediately upglacier from the continuously debris-covered zone (Fyffe et al., 2014). Thus,
329 | relatively high discharges of meltwater are focused into the troughs in the ~~mid-part of the~~
330 | glacier central ablation area, amplifying discharges flowing into the cluster of moulins at
331 | S12-S15 (Fig. 5). This explains the relatively large Q_s and u_s measured at S12 and S14 (Sect.
332 | 4.2).

333 Surface relief decreases downglacier due to the gravitational redistribution of debris down
334 moraine flanks into the troughs. This inverts relief development by reversing the ablation
335 gradient down the moraine flanks, reducing the systematic spatial variation in debris
336 thickness, and eventually resulting in the hummocky topography of the lower tongue (Fig. 4).
337 Consequently, there is less potential for the formation of an integrated channel network on
338 the continuously debris-covered zone, resulting in a chaotic, local stream network with
339 hollows which may lead to pond development. Consequently, catchments tend to be smaller
340 than upstream (Fig. 5), demonstrating that continuous debris cover can constrain catchment
341 size. Melt beneath a continuous debris cover is less than that of clean or dirty ice, in 2010
342 averaging 0.019 m w.e. d⁻¹ under continuous cover compared to, 0.025 m w.e. d⁻¹ and 0.047 m
343 w.e. d⁻¹ for clean and dirty ice respectively (Fyffe et al., 2014). Therefore, much less
344 meltwater is produced on the lower glacier, despite the lower elevation and warmer air
345 temperatures. This explains the small Q_s and slow u_s of the streams on the lower tongue.

346 **5.2 Establishment of channelized system draining upper glacier surface** 347 **streams**

348 Fast, peaked and low dispersion dye return traces from the upper glacier indicate that a
349 channelized system connects surface streams originating on clean and dirty ice, above the
350 continuously debris-covered zone, to the proglacial stream. This was the case even in early
351 June 2010 when the glacier was snow-covered well below the elevation of the upper moulins.

352 It is widely accepted that the seasonal evolution of a temperate glacier's hydrological system
353 is caused by an increase in the magnitude and amplitude of inputs into the system, initiated
354 by the switch from snow to ice melt, which causes pressure fluctuations large enough to
355 destabilise the hydraulically inefficient distributed system into a more efficient discrete
356 channel system (e.g. Nienow et al., 1998; Willis et al., 2002; Campbell et al., 2006). The
357 question of how a channelized network draining the upper glacier moulins could be
358 established prior to the depletion of the winter snow cover could be explained by two factors:
359 a) the channels did not completely close over the winter; or b) early season snowmelt inputs
360 were sufficiently large. Both of these possibilities will be evaluated in turn.

361 Conduit closure calculations estimate that the main conduit system is likely to have closed
362 over the winter (Appendix A). Although there is some uncertainty in the ice thickness values,
363 the modelling suggested it would take only 6-9 days for the conduits emanating from S12 and
364 S14 to close, depending upon the ice density and whether they fed into separate or one

365 combined conduit. Furthermore, if the subglacial conduit was broad and low rather than
366 semi-circular (as suggested by the form of the proglacial stream outlet), closure rates would
367 be faster than those estimated (Hooke et al., 1990).

368 It is therefore more likely that early season snowmelt inputs were able to cause
369 channelization. This could be due to the large catchment areas upstream of the moulins in the
370 central ablation area, with the flow concentrated by the topography into relatively large
371 streams (Sect. 5.1). The S12 and S14 catchments exist at a relatively low elevation (2400-
372 2500 m a.s.l.), below the terminus elevations of most clean glaciers in the western European
373 Alps. These factors could combine to result in inputs which were sufficiently large to
374 channelize the system, even from snowmelt. However, a channelized system can form when a
375 snowpack is still present if the snowpack remains longerrelatively late into the melt season
376 (Mair et al., 2002). This allows time for snowmelt percolation to become rapid enough to
377 develop an efficient supraglacial drainage system at the base of the snowpack, generating
378 input hydrographs with sufficient amplitude to channelize the system (Mair et al., 2002).

379 ~~Runoff generated by the large catchment areas supplying the S12 and S14 moulins combined~~
380 ~~with topographic flow concentration (Sect. 5.1) could produce input discharges large enough~~
381 ~~to initialise channelization, even from snowmelt. In early June of both years a large~~
382 ~~supraglacial stream was observed flowing beneath or through the snow cover in the valley to~~
383 ~~the east of the central moraine above the S12-S14 moulins. The S12-S14 catchments exist at~~
384 ~~a relatively low elevation (2400-2500 m a.s.l.), below the terminus elevations of most clean~~
385 ~~glaciers in the western European Alps. Consequently, favourable spring weather conditions~~
386 ~~could lead to water inputs large enough to destabilise the distributed system. As suggested by~~
387 ~~Mair et al. (2002), a channelized system could form when a snow pack is still present if the~~
388 ~~snowpack remains longer into the melt season. This allows time for snowmelt percolation to~~
389 ~~become rapid enough to develop an efficient supraglacial drainage system at the base of the~~
390 ~~snowpack, generating input hydrographs with sufficient amplitude to channelize the system.~~

391 **5.3 Evolution of channelized system over the summer**

392 The u of traces from the upper glacier moulins in 2011 (S12, S14 and S15) remained higher
393 than those from the lower glacier (S5 and S7) throughout the season (Fig. 10a). However,
394 compared to June, the late July return curves S12_30Jul0711 and S14_29Jul0711 were
395 slower and more dispersed, although they still had singleular peaks (Figs. 7d and 7e,
396 respectively) - Surprisingly, this indicat~~ing~~es the efficiency of the channel system had

397 reduced since June. In contrast, the early August traces into upper glacier moulins S12, S14
398 and S15 in 2011 all showed a strong increase in u (Fig. 10a), a decrease in D and b , and an
399 increase in A_m (Fig. 10b), compared to the return curves prior to 31 ~~July /07/2011~~.

400 ~~Normally, it~~ would be expected that increased melt inputs between the early and mid-
401 ablation season would ~~result in increase the efficiency of the in a progressively more efficient~~
402 channel network, ~~with any variations from this trend a result of weather fluctuations.~~ The
403 slower and more dispersed July traces could be due to increased conduit roughness, caused
404 by a smaller discharge allowing boulders and cobbles on the conduit floor to decrease flow
405 velocity (Gulley et al., 2012). However June and July proglacial discharges were similar and
406 the degree of dispersion seen was less in June. Rapid changes in ~~flow velocity~~ transit velocity
407 can also result from inflow modulation and/or changes in the channel geometry (Nienow et
408 al., 1996; Schuler and Fischer, 2009). However similar patterns were observed at three
409 different moulins traced at similar times on different days (Table 4), ~~so it is unlikely that a~~
410 diurnal increase in the supraglacial input discharges, resulting in inflow modulation of the
411 tracer transit velocity, so it is unlikely that inflow modulation over short time periods was the
412 cause of the differences between the July and August traces. More plausible is that cold
413 weather between 17 ~~and 27 July /07/2011 and 27/07/2011~~ (Fig. 2b, maximum daily
414 temperatures were generally below 10°C, and air temperatures fell below zero at UWS during
415 the mornings of 24 ~~and 25 July /07/2011 and 25/07/2011~~) and reduced meltwater inputs
416 resulted in relative closure of the main subglacial conduit (Röthlisberger, 1972). When the
417 weather warmed from 28 ~~July /07/2011~~ the system was not able to efficiently evacuate the
418 increased discharges, resulting in hydraulic damming (caused by the conduit geometry being
419 small relative to the flow through the conduit), and the slower u and greater D observed in
420 July. In this case the hydraulic damming was caused by changes in the channel geometry
421 rather than diurnal variations of supraglacial or proglacial discharge. This interpretation is
422 corroborated by an observed increase in glacier sliding velocities over the same period, likely
423 generated by high basal water pressure as water was forced across large areas of the bed
424 (Fyffe, 2012). Conduit diameters likely grew rapidly so that by August the network could
425 accommodate the increased discharges.

426 The September 2011 traces into the upper glacier moulins (Fig. 7d-f), suggested the drainage
427 system remained more efficient than in late July but slightly less efficient than in early
428 August. Air temperatures remained high throughout August 2011 (mean LWS air temperature
429 in July was 9.4°C, but 12.6°C in August 2011), and proglacial discharges were all higher in

430 September 2011 than they were during any earlier traces (Table 4), explaining the
431 preservation of drainage system efficiency. S12b and S14b u in September 2010 was slower
432 than its 2011 counterparts (Figs. 7d and e). Air temperatures during August and September
433 (until 10 ~~September /09/2011~~) were much cooler in 2010 compared to 2011 (see Fig. 2).
434 Consequently, input discharges in September 2010 would have been smaller than in 2011,
435 increasing conduit closure rates and slowing water velocities.

436 **5.4 Englacial and subglacial drainage beneath continuous debris**

437 The drainage system beneath the continuously debris-covered zone was far less efficient than
438 the upper debris-free area. Traces into S1, S3, S5 and S7 had slower u and in some cases
439 (especially S5 and S7, Figs. 7b and c) displayed multiple peaks, indicating the water spent at
440 least some time within a less efficient hydrological network, ~~with multiple flow paths~~
441 ~~characteristic of a distributed system.~~ The multi-peaked nature of the early June traces into S5
442 and S7 does suggest the existence of a distributed system emanating from these streams. The
443 traces were also particularly broad and had low velocities, although it is the large number of
444 small peaks in these early traces (there are at least 7 distinct peaks in the S7_05Jun11 and
445 S5_06Jun11 curves) which suggests the system was distributed. Breakthrough curves with
446 slow μ and large D and b values have been returned in previous studies, even though the
447 system has been channelized, due to variations in supraglacial and main channel discharge
448 (Nienow et al., 1996; Schuler et al., 2004; Werder et al., 2010) or an increase in roughness
449 (Gulley et al., 2012). However curves from these studies (where shown) still exhibited one
450 main peak, although they may have a shoulder or small secondary peak. The only
451 breakthrough curves in the literature which are comparable to S7_05Jun11 and S5_06Jun11
452 are those from boreholes (e.g. Hooke and Pohjola, 1994), although monitoring of the
453 borehole injections continued for much longer after injection. It is therefore likely that the S5
454 and S7 streams were draining into some kind of distributed system, at least early in the melt
455 season. On average, injection points S8 and below had a relatively slow average u of 0.26 m
456 s^{-1} , and a low average P_r of 348%.

457 Traces into S3, S5 and S7 showed evidence of drainage system evolution (Figs. 7a-c).
458 Certain peaks of the dye breakthrough curves became more prominent or coalesced over the
459 season, suggesting certain flow paths began to dominate within a more integrated network.
460 Therefore the hydrological network did increase in efficiency, but not to the extent that water
461 was transferred as quickly as from the upper glacier moulins. Later in the season there was
462 evidence that the efficiency of the hydrological network decreased, e.g. a decrease in u and

Formatted: Font: Italic

Formatted: Font: Italic, Underline

Formatted: Font: Italic

Formatted: Font: Italic

463 increase in D (S3), or a return to traces with multiple peaks (S5, Fig. 7b), indicating increased
464 flow divergence and the reversion of the system back to the distributed configuration found
465 early in the season.

466 The role of debris in reducing meltwater inputs below the critical discharge at which channels
467 develop (Hewitt and Fowler, 2008) appears crucial in inhibiting channelisation. Low ablation
468 rates (around $0.02 \text{ m w.e. d}^{-1}$, Fyffe et al., 2014), and an attenuated melt signal under thick
469 debris result in small and likely low-amplitude supraglacial stream discharges (Sect. 5.1).
470 Furthermore, the uneven topography of the lower glacier (Figs. 4 and 5) inhibits dendritic
471 drainage system development and results in small supraglacial catchments and consequently
472 smaller but more numerous inputs to the englacial system. These low magnitude and
473 amplitude meltwater inputs can be accommodated within a less efficient glacial drainage
474 system.

475 It is also possible that the larger moraines could create local areas of high subglacial
476 hydraulic potential, creating barriers to subglacial flow (Fischer et al., 2005). This could
477 increase the complexity of the subglacial drainage system beneath hummocky debris and
478 increase the length of the drainage pathways leading to the channelized system.

479 These results imply the coexistence of an inefficient drainage system beneath the
480 continuously debris-covered zone with an efficient channelized system which emanates from
481 the upper glacier. Distributed and channelized systems are known to coexist, for instance on
482 Haut Glacier d'Arolla away from the preferential axis of drainage (Nienow et al., 1996), on
483 the western side of Midtalsbreen, southern Norway (Willis et al., 1990), and within the
484 smaller drainage catchment of the South Cascade Glacier, USA (Fountain, 1993), but
485 unusually on Miage Glacier the distributed system occurs downglacier of the channelized
486 network and is the main system of transferring melt on the lower glacier, even though a
487 conduit system exists within the same drainage catchment. However, the proportional
488 distance water has travelled in the efficient and less efficient systems is not known and the
489 systems may not merge until close to the snout.

490 On the lower glacier it is envisaged that the link between the supraglacial stream and the
491 main subglacial channel is the inefficient part of the system. It is this part which causes the
492 lower u and multi-peaked traces. Borehole experiments at Haut Glacier d'Arolla (Hubbard et
493 al., 1995) revealed an area of distributed drainage adjacent to the main channel which
494 supplied water to, and was the recipient of, water from the main channel, depending upon the

495 direction of the pressure gradient between the two areas. A distributed and channelized
496 system probably occurs simultaneously under Miage Glacier, with the distributed system
497 draining to the main channel system. Unlike the system described by Hubbard et al. (1995),
498 water enters the Miage Glacier distributed system from the surface so it contains water
499 irrespective of the pressure gradient between the channel and distributed system.

500 Sediment layers are commonly found beneath debris-covered glaciers, due to high rates of
501 sediment supply (Maisch et al., 1999; Hewitt, 2014). It is likely that a layer of sediment
502 underlies the lower glacier (Pavan et al., 1999, cited in Deline, 2002), and if this is thick and
503 highly porous it will likely further inhibit conduit formation, since a sediment wedge
504 downglacier of a hard bed can stall channelisation (Flowers, 2008).

505 **6 Conclusions**

506 This is the first extensive investigation of the structure and seasonal evolution of the
507 hydrological system of a debris-covered glacier using dye tracing techniques.

508 Forty-eight dye injections were conducted into 16 surface streams distributed across both
509 debris-free and debris-covered areas of Miage Glacier over the 2010 and 2011 summers. The
510 return curves were analysed in conjunction with supraglacial stream discharge measurements,
511 meteorological data, proglacial stream discharges and topographical analysis of a DEM. The
512 main findings are that:

- 513 1. The upper ablation zone, exhibiting patchy debris cover and high surface melt rates, is
514 connected to the main proglacial stream via an efficient channelized system, which is
515 established early in the season when snow-cover is still extensive, and maintained
516 throughout the ablation season.
- 517 2. The majority of meltwater from the lower continuously debris-covered area is drained
518 via an inefficient network which may feed gradually into the main channelized
519 network, although on occasion streams make a direct connection with the main
520 conduit system.
- 521 3. Significant and rapid changes in capacity and efficiency of the main channelized
522 network may occur mid-season in response to meltwater supply fluctuations.
- 523 4. Although the drainage network beneath the continuously debris-covered zone
524 increased in efficiency between the early and mid-season, it did not become as
525 efficient as the upglacier system.

526 5. The spatial distribution of debris influences the development of the hydrological
527 system in important and contrasting ways, through its influence on both melt rates and
528 surface topography. First, the establishment and maintenance of an efficient
529 channelized network emanating from moulins draining the upper ablation zone is
530 promoted both by very high ablation rates on patchy debris and dirty-ice areas and the
531 topographic concentration of flow into large channels within the moraine troughs.
532 This topographic enhancement is a direct consequence of the large difference in melt
533 rates between medial moraines, which are insulated by thick debris, and the high melt
534 rates of the dirty ice in the intermoraine valleys. Second, the small discharges and low
535 amplitude hydrographs of streams draining the continuously debris-covered area
536 result from both low and attenuated melt peaks beneath thick debris and the
537 hummocky topography which restricts catchment and stream size. This produces
538 dispersed low magnitude melt inputs, preventing water pressure fluctuations
539 becoming great enough to destabilize the distributed system beneath.

540

541 These interpretations contrast with conclusions from similar dye tracing studies conducted on
542 debris-free glaciers. In particular, on Miage Glacier: i) the formation of the channelized
543 network is not related to the position of the snowline and ii) u increased linearly, rather than
544 decreased with distance upglacier. This means that the hydrological evolution of extensively
545 debris-covered glaciers is distinct from that of clean glaciers.

546 These findings have implications for those glaciers which are becoming increasingly debris
547 covered (Bolch et al., 2008; Bhambri et al., 2011; Lambrecht et al., 2011) since the debris is
548 likely to influence melt water travel times and therefore the proglacial runoff signal. Debris
549 thickness and spatial extent at Miage Glacier is similar to debris-covered glaciers in mountain
550 ranges such as the Himalayas (Rounce and McKinney, 2014; Schauwecker et al., 2015) and
551 Alaska (Kienholz et al., 2015) hence these findings have relevance to regions where debris-
552 covered glaciers are extensive and common.

553 **Appendix A: Conduit Closure Rates**

554 Conduit closure rates were calculated by integrating equation 7 in Hooke (1984, cited in
555 Nienow *et al.*, 1998). The time, t (s) for a conduit to close to a given radius, r_r (m) is given
556 by:

557

558
$$t = \frac{\ln(r_r) - \ln(r_i)}{\left(\frac{\rho_i g h}{n A_G}\right)^3}, \quad (\text{A1})$$

559
 560 where ρ_i is the ice density (kg m^{-3}), g is gravitational acceleration (9.81 ms^{-2} ; ~~Oke (1978)~~), n
 561 = 3 and $A_G = 5.8 \times 10^{-7} \text{ Pa s}^{-1/30.5}$, both constants in Glen's flow law (Nienow et al., 1998).
 562 The ice thickness (h , m) was derived from the ice thickness map (see Sect. 3.3) by extracting
 563 a profile of thickness measurements (at approximately 25 m intervals) from the proglacial
 564 stream portal, up the northern lobe and along the glacier centreline. It was assumed that a
 565 single conduit links the upper moulins and proglacial stream, with the initial conduit radius
 566 (r_i , m) derived by linearly interpolating the measured input (see below) and proglacial stream
 567 discharge, and dividing this by u to give the channel cross sectional area along the entire
 568 stream length. The assumption of a single subglacial conduit allows the closure calculations
 569 to be applied to the likely maximum conduit cross-sectional area and should not be taken to
 570 imply that this is the most likely drainage structure. The conduit was assumed to be semi-
 571 circular and to have effectively closed when it had a radius of 0.01 m.

572 To understand the sensitivity of the calculations to r_i , the time taken for the conduit to close
 573 was calculated using either the S12, S14 or the sum of the S12 and S14 September 2011
 574 supraglacial discharges. The proglacial discharge was taken as the mean of the proglacial
 575 discharge at the injection and peak of the return curve for the respective trace, or the mean for
 576 the combined S12 and S14 test. The ice density was also varied from 830 kg m^{-3} (lowest
 577 density of glacial ice (Paterson, 1994)) to 920 kg m^{-3} (pure ice at 0°C , Oke (1978)).

578 In all simulations the largest distance from the gauging station at which the conduits would
 579 take 4 months to close was between 1820 m and 1844 m, around 3 km downglacier of S12
 580 and S14. It was calculated that the ice would need to be 144 to 160 m thick (depending upon
 581 the ice density) in order for a combined S12 and S14 conduit to take 4 months to close,
 582 whereas the ice thickness calculated using the VDA DEM at the elevation of the S12 and S14
 583 moulins was 375 to 380 m.

584 Acknowledgements

585 The authors would like to thank two anonymous reviewers for their thoughtful and
 586 constructive comments. This work was performed while C. Fyffe was in receipt of a
 587 studentship from the School of the Environment, University of Dundee. The authors thank

Formatted: Not Superscript/ Subscript

588 the University of Worcester for kindly funding the publication of this paper. The authors
589 would like to thank J. Holden for the loan of a Seapoint Rhodamine fluorometer and P.
590 Nienow for advice on performing dye tracing studies. F. Brunier from Regione Autonoma
591 Valle d'Aosta kindly provided air pressure data from Mont de la Saxe. Students from the
592 University of Dundee, Northumbria University, Aberdeen University and Cambridge
593 University as well as L. Gilbert provided invaluable help in the field. C. Thomas provided
594 assistance with conduit closure calculations. We would also like to thank M. Vagliasindi and
595 J.P. Fosson of Fondazione Montagna Sicura for excellent logistical support at the field site.
596 The VDA DEM was kindly provided by Regione Autonoma Valle d'Aosta (Modello
597 Altimetrico Digitale della Regione Autonoma Valle d'Aosta aut. n. 1156 del 28.08.2007).

598 **References**

- 599 Arnold, N. S.: A new approach for dealing with depressions in digital elevation models when
600 calculating flow accumulation values, *Prog. Phys. Geog.*, 34(6), 781–809, 2010.
- 601 Bhambri, R., Bolch, T., Chaujar, R.K. and Kulshreshtha, S.C.: Glacier changes in the
602 Garhwal Himalaya, India, from 1968 to 2006 based on remote sensing, *J. Glaciol.*,
603 57(203), 543–556, 2011.
- 604 Bolch, T., Buchroithner, M., Pieczonka, T. and Kunert, A.: Planimetric and volumetric
605 glacier changes in the Khumbu Himal, Nepal, since 1962 using Corona, Landsat TM
606 and ASTER data, *J. Glaciol.*, 54(187), 592–600, 2008.
- 607 Bolch, T., Kulkarni, A., Kääb, A., Huggel, C., Paul, F., Cogley, J. G., Frey, H., Kargel, J. S.,
608 Fujita, K., Scheel, M., Bajracharya, S. and Stoffel, F.: The state and fate of Himalayan
609 glaciers, *Science*, 336(6079), 310–314, 2012.
- 610 Brock, B., Mihalcea, C., Kirkbride, M., Diolaiuti, G., Cutler, M. and Smiraglia, C.:
611 Meteorology and surface energy fluxes in the 2005-2007 ablation seasons at Miage
612 debris-covered glacier, Mont Blanc Massif, Italian Alps, *J. Geophys. Res.*, (115)
613 D09106, 2010.
- 614 Campbell, F. M. A., Nienow, P. W. and Purves, R. S.: Role of the supraglacial snowpack in
615 mediating meltwater delivery to the glacier system as inferred from dye tracer
616 investigations, *Hydrol. Process.*, (20), 969-985, 2006.
- 617 Carabelli: [Seismic survey 1957] Rilevamenti di ghiacciai e studi glaciologici in occasione
618 dell'anno geofisico (Ghiacciaio del Miage): eslanazione geofisica. *Bollentino del*
619 *Comitato Glaciologico Italiano*, 9(1), 87-94, 1961.

620 Casati, D.: Studio della dinamica di un debris-covered glacier: il Ghiacciaio del Miage. Tesi
621 Laurea, Universita Milano, 249, 1998.

622 Deline, P.: Etude géomorphologique des interactions écroulements rocheux/glaciers dans la
623 haute montagne alpine (verant sud-est du Massif du Mont Blanc), PhD thesis, 2002.

624 Deline, P.: Interactions between rock avalanches and glaciers in the Mont Blanc massif
625 during the late Holocene, *Quaternary Sci. Rev.*, (28), 1070-1083, 2009.

626 Deline, P., Gardent, M., Kirkbride, M. P., Le Roy, M. and Martin, B.: Geomorphology and
627 dynamics of supraglacial debris covers in the Western Alps, *Geophysical Research*
628 *Abstracts*, EGU General Assembly 2012, (14), 2012.

629 Dingman, S. L.: *Physical Hydrology* Second Edition, Prentice Hall, New Jersey, 2002.

630 Diolaiuti G., D'Agata C., Meazza A., Zanutta A. and Smiraglia C.: Recent (1975-2003)
631 changes in the Miage debris-covered glacier tongue (Mont Blanc, Italy) from analysis
632 of aerial photos and maps. *Geografia Fisica e Dinamica Quaternaria*, (32), 117-127,
633 2009.

634 [Fischer, U. H., Braun, A., Bauder, A. and Flowers, G. E.: Changes in geometry and](#)
635 [subglacial drainage derived from digital elevation models: Unteraargletscher,](#)
636 [Switzerland, 1927-97. *Ann. Glaciol.*, \(40\), 20-24, 2005.](#)

637 Flowers, G. E.: Subglacial modulation of the hydrograph from glacierized basins, *Hydrol.*
638 *Process.*, (22), 3903-3918, 2008.

639 Foster, L. A., Brock, B. W., Cutler, M. E. J. and Diotri F.: A physically based method for
640 estimating supraglacial debris thickness from thermal band remote sensing data, *J.*
641 *Glaciol.*, 58(210), 677-691, 2012.

642 Fountain, A. G.: Geometry and flow conditions of subglacial water at South Cascade Glacier,
643 Washington State, U.S.A.; an analysis of tracer injections, *J. Glaciol.*, 39(131), 143-
644 156, 1993.

645 Fyffe, C. L.: The hydrology of debris-covered glaciers, University of Dundee, PhD Thesis,
646 2012.

647 Fyffe, C. L., Reid, T. D., Brock, B. W., Kirkbride, M. P., Diolaiuti, G., Smiraglia, C. and
648 Diotri, F.: A distributed energy-balance melt model of an alpine debris-covered
649 glacier, *J. Glaciol.*, 60(221), 587-602, 2014.

650 Gulley, J. and Benn, D. I.: Structural control of englacial drainage systems in Himalayan
651 debris-covered glaciers, *J. Glaciol.*, 53(182), 399-412, 2007.

652 Gulley, J. D., Walthard, P., Martin, J., Banwell, A. F., Benn, D. I., Catania, G.: Conduit
653 roughness and dye-trace breakthrough curves: why slow velocity and high

654 dispersivity may not reflect flow in distributed systems, *J. Glaciol.*, 58(211), 915-925,
655 2012.

656 Hallet, B., Lorrain, R. and Souchez, R.: Rates of erosion and sediment evacuation by glaciers:
657 a review of field data and their implications, *Global Planet. Change*, (12), 213-235,
658 1996.

659 Hasnain, S. I., Jose, P. G., Ahmad, S. and Negi, D. C.: Character of the subglacial drainage
660 system in the ablation area of Dokriani glacier, India, as revealed by dye-tracer
661 studies, *J. Hydrol.*, (248), 216-223, 2001.

662 Hewitt, I. J. and Fowler, A. C.: Seasonal waves on glaciers, *Hydrol. Process.*, (22), 3919–
663 3930, 2008.

664 Hewitt, K.: *Glaciers of the Karakoram Himalaya: Glacial Environments, Hazard and*
665 *Resources*, Springer, Dordrecht, 2014.

666 Hooke, R. LeB.: On the role of mechanical energy in maintaining subglacial water conduits
667 at atmospheric pressure, *J. Glaciol.*, (30), 280-287, 1984.

668 Hooke, R. LeB., Laumann, T. and Kohler, J.: Subglacial water pressures and the shape of
669 subglacial conduits, *J. Glaciol.*, 36(122), 67-71, 1990.

670 [Hooke, R. LeB. and Pohjola, V. A.: Hydrology of a segment of a glacier situated in an](#)
671 [overdeepening, Storglaciären, Sweden, *J. Glaciol.*, 40\(134\), 140-148, 1994.](#)

672 Hubbard, B. P., Sharp, M. J., Willis, I. C., Nielsen, M. K. and Smart, C. C.: Borehole water-
673 level variations and the structure of the subglacial hydrological system of Haut
674 Glacier d’Arolla, Valais, Switzerland, *J. Glaciol.*, 41(139), 572-583, 1995.

675 ~~Kiein~~ Kieinholz, C., Herreid, S., Rich, J. L., Arendt, A. A., Hock, R. and Burgess E. W.:
676 Derivation and analysis of a complete modern-date glacier inventory for Alaska and
677 northwest Canada. *J. Glaciol.*, 61(227), 403-420, 2015.

678 Kilpatrick, F. A. and Cobb, E. D.: *Measurement of discharge using tracers*, United States
679 Government Printing Office, Washington, 1985.

680 Kirkbride, M.P. and Deline, P.: The formation of supraglacial debris covers by primary
681 dispersal from transverse englacial debris bands. *Earth Surf. Proc. Land.*, (38), 1779-
682 1792, 2013.

683 Kirkbride, M. P. and Dugmore, A. J.: Glaciological response to distal tephra fallout from the
684 1974 eruption of Heckla, south Iceland, *J. Glaciol.*, 49(166), 420-428, 2003.

685 Lambrecht, A., Mayer, C., Hagg, W., Popovnin, V., Rezepkin, A., Lomidze, N. and
686 Svanadze, D.: A comparison of glacier melt on debris-covered glaciers in the northern

687 and southern Caucasus. *The Cryosphere*, (5), 525-538, doi: 10.5194/tc-5-525-2011,
688 2011.

689 Lejeune, Y., Bertrand, J-M., Wagnon, P. and Morin, S.: A physically-based model of the
690 year-round surface energy and mass balance of debris-covered glaciers. *J. Glaciol.*,
691 59(214), 327-344, 2013.

692 Lesca, C.: Emploi de la photogrammétrie analytique pour la détermination de la vitesse
693 superficielle des glaciers et des profondeurs relatives, *Bollettino del Comitato*
694 *Glaciologico Italiano*, (22), 169-186, 1974.

695 Mair, D., Nienow, P., Sharp, M. J., Wohlleben, T. and Willis, I.: Influence of subglacial
696 drainage system evolution on glacial surface motion: Haut Glacier d'Arolla,
697 Switzerland, *J. Geophys. Res.*, 107(B8), EPM 8-1–EPM 8-13, doi:
698 10.1029/2001JB000514, 2002.

699 Maisch, M., Haerberli, W., Hoelzle, M. and Wenzel, J.: Occurrence of rocky and sedimentary
700 glacier beds in the Swiss Alps as estimated from glacier-inventory data. *Ann. Glaciol.*,
701 (28), 231-235, 1999.

702 Mattson, L. E., Gardener, J. S. and Young, G. J.: Ablation on debris covered glaciers: an
703 example from the Rakhiot Glacier, Punjab, Himalaya, *Snow and Glacier Hydrology*,
704 *IAHS Publication*, (218), 289-296, 1993.

705 Maurya, A. S., Shah, M., Deshpande, R. D., Bhardwaj, R. M., Prasad, A. and Gupta, S. K.:
706 Hydrograph separation and precipitation source identification using stable water
707 isotopes and conductivity: River Ganga at Himalayan foothills, *Hydrol. Process.*, (25),
708 1521-1530, 2011.

709 Nicholson, L. and Benn, D. I.: Calculating ice melt beneath a debris layer using
710 meteorological data, *J. Glaciol.*, 52(178), 463-470, 2006.

711 Nienow, P. W., Sharp, M. and Willis, I. C.: Velocity-discharge relationships derived from
712 dye-tracer experiments in glacial meltwaters: implications for subglacial flow
713 conditions, *Hydrol. Process.*, (10), 1411-1426, 1996.

714 Nienow, P. W., Sharp, M. and Willis, I. C.: Seasonal changes in the morphology of the
715 subglacial drainage system, Haut Glacier d'Arolla, Switzerland, *Earth Surf. Proc.*
716 *Land.*, (23), 825-843, 1998.

717 Oke, T. R.: *Boundary Layer Climates*, Methuen and Co. Ltd., London, 1978.

718 Østrem, G.: Ice melting under a thin layer of moraine, and the existence of ice cores in
719 moraine ridges, *Geogr. Ann.*, 41(4), 228-230, 1959.

720 Paterson, W. S. B.: The Physics of Glaciers, Third Edition, Butterworth-Heinemann, Oxford,
721 1994.

722 Pavan, M., Smiraglia, C. and Merlanti, F.: Prospezione geofisica sul ghiacciaio del Miage
723 (Alpi occidentali), Poster, Genova, 1, 1999.

724 Reid, T. D. and Brock, B. W.: Assessing ice-cliff backwasting and its contribution to total
725 ablation of debris-covered Miage glacier, Mont Blanc massif, Italy, *J. Glaciol.*,
726 60(219), 3-13, doi: 10.3189/2014JoG13J045, 2014.

727 Röthlisberger, H.: Water pressure in intra- and subglacial channels, *J. Glaciol.*, 11(62), 177-
728 203, 1972.

729 Rounce, D. R. and McKinney, D. C.: Debris thickness of glaciers in the Everest area (Nepal
730 Himalaya) derived from satellite imagery using a nonlinear energy balance model,
731 *The Cryosphere*, (8), 1317–1329, 2014.

732 Schauwecker, S., Rohrer, M., Huggel, C., Kulkarni, A., Ramanathan, A., Salzmann, N.,
733 Stoffel, M., Thayyen, R. and Brock, B.: Remotely sensed debris thickness mapping of
734 Bara Shigri Glacier (Indian Himalayas), *J. Glaciol.* ,61(228), 675-688, 2015.

735 Scherler, D., Bookhagen, B. and Strecker, M. R.: Spatially variable response of Himalayan
736 glaciers to climate change affected by debris cover. *Nat. Geosci.*, 4(3), 156-159, 2011.

737 Schuler, T. V. and Fischer, U. H.: Modeling the diurnal variation of tracer transit velocity
738 through a subglacial channel, *J. Geophys. Res.*, (144), F04017, 2009.

739 [Schuler, T., Fischer, U. H. and Gudmundsson, G. H.: Diurnal variability of subglacial](#)
740 [drainage conditions as revealed by tracer experiments, *J. Geophys. Res.*, \(109\),](#)
741 [F02008, doi: 10.1029/2001JF000082, 2004.](#)

742 Seaberg, S. Z., Seaberg, J. Z., Hooke, R. LeB. and Wiberg, D. W.: Character of the englacial
743 and subglacial drainage system in the lower part of the ablation area of Storglaciären,
744 Sweden, as revealed by dye-trace studies, *J. Glaciol.*, (34), 217-227, 1988.

745 Stokes, C. R., Popovnin, V., Aleyhikov, A., Gurney, S. D. and Shahgedanova, M.: Recent
746 glacier retreat in the Caucasus Mountains, Russia, and associated increase in
747 supraglacial debris cover and supra-/proglacial lake development, *Ann. Glaciol.*, (46),
748 195-203, 2007.

749 [Werder, M. A., Schuler, T. V. and Funk, M.: Short term variations of tracer transit speed on](#)
750 [alpine glaciers. *The Cryosphere*, \(4\), 381-396, 2010.](#)

751 Willis, I. C., Arnold, N. S. and Brock, B. W.: Effect of snowpack removal on energy balance,
752 melt and runoff in a small supraglacial catchment, *Hydrol. Process.*, (16), 2721-2749,
753 2002.

- 754 Willis, I. C., Sharp, M. J. and Richards, K. S.: Configuration of the drainage system of
755 Middalsbreen, Norway, as indicated by dye-tracing experiments, *J. Glaciol.*, 36(122),
756 89-101, 1990.
- 757 Xu, J., Grumbine, R. E., Shrestha, A., Eriksson, M., Yang, X., Wang, Y. and Wilkes, A.: The
758 Melting Himalayas: Cascading Effects of Climate Change on Water, Biodiversity, and
759 Livelihoods, *Conserv. Biol.*, 23(3), 520-530, 2009.

760 Table 1 Details of supraglacial and proglacial stream instruments.

Quantity	Location	Time period	Manufacturer	Type	Accuracy
Stage	Proglacial	2010 and June 2011	GE Sensing	Druck PTX1830 (vented)	±0.1% full scale (or ±0.06% full scale)
	Proglacial	Aug and Sep 2011	Onset	HOBO U20 - 001-04 (non- vented)	±0.075% full scale, ±0.3 cm
Fluorescence	Proglacial	2010 and June 2011	Seapoint	Rhodamine fluorometer	Not stated but minimum detection 0.02 ppb
	Proglacial	July, Aug, Sep 2011	Turner	Cyclops-7 Rhodamine	Not stated but minimum detection 0.01 ppb
Conductivity	Supraglacial	2010 and 2011	Hanna	HI9033 with HI 76302W probe	± 1% full scale (excluding probe)

761

762

763 Table 2 Parameters calculated for each dye breakthrough curve.

Symbol	Unit	Definition
u	ms^{-1}	The minimum estimate of the average flow velocity <u>transit velocity of the tracer through the hydrological system</u> (d/t).
d	m	The straight line distance from the gauging station to the injection site. Due to the bend in the glacier above S4, for all traces above this point the distance between the injection point and S4 was used and added to the distance between S4 and the gauging station to give the total distance.
t	s	The time between the injection and peak of the return curve.
D	$\text{m}^2 \text{s}^{-1}$	The dispersion coefficient, which is a measure of the spread of the dye as it travels through the glacier, see <u>text for details</u> . Seaberg (1988, equation 4).
b	m	The dispersivity, calculated as D/u (Seaberg, 1988, p 224).
A_m	m^2	The apparent mean cross-sectional area, calculated as Q_m/u .
Q_m	$\text{m}^3 \text{s}^{-1}$	The mean discharge between the injection and detection point, calculated as the average of the supraglacial (assumed constant) and proglacial (average of the discharge at the injection and peak of the return curve) discharge.
P_r	%	<u>The percentage dye return $((V_r/V_i)*100)$.</u>
V_r	ml	The - volume of dye recovered, <u>see text for details</u> . calculated from the equation below, which was derived from the equation to calculate discharge given by Kilpatrick and Cobb (1985, p6):
$V_r = \frac{S^{-1} \left(\frac{1}{1.649 \times 10^{-8}} (Q_p A_e) \right)}{\epsilon_{di}}$		
S	n/a	The specific gravity of the dye used (1.15 for rhodamine WT).
Q_p	$\text{m}^3 \text{s}^{-1}$	The average proglacial discharge from the time of injection until the time of the peak of the dye return curve.
A_e	ppb minute ⁺	The area under the dye breakthrough curve.
ϵ_{di}	ppb	The concentration of the dye prior to injection.
P_r	%	The percentage dye return $((V_r/V_i)*100)$.
V_i	ml	The volume of dye injected.

764

765

766 | **Table 3 Mean supraglacial discharges (Q_s) and velocities (u_s) for the 2011 streams.**

Name	Q_s ($m^3 \cdot s^{-1}$)	u_s (ms^{-1})
S5	0.030	0.17
S7	0.019	0.24
S12	0.177	0.46
S14	0.622	1.52
S15	0.017	0.36

Table 3. Dye trace parameters for all injection points in 2010, for definitions see Table 2. *Only part of the rising limb of the trace was returned. Mean P_r does not include values >100%, which can be caused by error in Q_p or variations in the background fluorescence which alters A_c .

Name	Date	<i>Time</i>	V_i	Trace?	u	D	b	Q_p	A_c	P_r
			(ml)		(m s ⁻¹)	(m ² s ⁻¹)	(m)	(m ³ s ⁻¹)	(ppb minute ⁻¹)	(%)
S1	<u>5 Jun</u> 05/06 /2010	<u>17:51:00</u>		N						
S2	<u>08 Jun</u> #06 /2010	<u>16:00:00</u>	40	N						
S6	<u>09 Jun</u> #06 /2010	<u>17:46:05</u>	40	Y	0.583	0.884	1.52	2.88	20.8	37.7
S8	<u>10 Jun</u> #06 /2010	<u>12:12:00</u>	120	Y	0.434	1.180	2.72	2.90	55.9	34.0
S13	<u>11 Jun</u> #06 /2010	<u>12:43:00</u>	200	Y	0.830	1.800	2.17	3.36	129.4	54.6
S1	<u>12 Jun</u> #06 /2010	<u>12:05:00</u>	40	Y	0.024	0.004	0.15	5.97	34.4	129.0
S10	<u>13 Jun</u> #06 /2010	<u>15:07:00</u>	160	Y	0.602	2.300	3.82	5.70	40.0	35.8
S3	<u>14 Jun</u> #06 /2010	<u>16:50:00</u>	80	Y	0.192	0.230	1.20	2.84	3.7	3.3
S9	<u>18 Jun</u> #06 /2010	<u>17:45:00</u>	120	N						

Formatted: Font: Italic

Formatted: Font: Italic, Subscript

S3	<u>19 Jun</u> #06/2010	<u>14:25:00</u>	80	N						
S5	<u>20 Jun</u> #06/2010	<u>13:21:30</u>	80	N						
S3	<u>29 Jul</u> #07/2010	<u>17:52:00</u>	80	Y	0.345	0.860	2.49	10.71	50.6	170.0
S5	<u>30 Jul</u> #07/2010	<u>16:15:00</u>	120	Y	0.226	9.490	42.01	5.63	47.4	55.9
S9	<u>31 Jul</u> #07/2010	<u>12:11:00</u>	120	N						
S11	<u>1 Aug</u> 01/08/2010	<u>11:32:00</u>	120	Y	0.442	3.550	8.03	7.80	56.3	91.8
S13	<u>03 Aug</u> #08/2010	<u>12:21:30</u>	160	N						
S16	<u>04 Aug</u> #08/2010	<u>12:01:00</u>	200	N						
S5b	<u>06 Aug</u> #08/2010	<u>16:10:00</u>	80	Y*				2.98		
S13	<u>05 Sep</u> #09/2010	<u>12:15:10</u>	160	N						
S14b	<u>06 Sep</u>	<u>14:30:30</u>	200	Y	0.613	1.770	2.89		181.9	

	/09/2010									
S3	<u>09 Sep</u>	<u>14:27:00</u>	80	Y	0.265	1.870	7.05	1.65	100.2	51.9
	/09/2010									
S4	<u>10 Sep</u>	<u>15:56:00</u>	80	N						
	/09/2010									
S12b	<u>11 Sep</u>	<u>15:47:00</u>	100	Y	0.318	7.800	24.55	1.93	141.5	68.6
	/09/2010									
Mean (all)					0.406	2.645	8.21	4.63	71.8	48.2
Mean (upper)					0.561	3.444	8.29	4.74	109.8	62.7
Mean (lower)					0.296	2.074	8.16	4.57	44.7	36.6

Table 4 Dye trace parameters for all 2011 dye injections. The Q_s and u_s type is either 'D', dilution gauging, 'V', the velocity area method (timing of floats), or 'AdD', adjusted to dilution gauging (see Sect. 3.1.2 for details). *Indicates traces with multiple peaks for which the D and b parameters are less reliable. **Only the first part of the trace was returned. ***A trace was returned but was poor quality so has not been interpreted. †The Q_s values are an estimate because the stream cross-sectional area could not be measured, in these cases the mean cross-sectional area was multiplied by the velocity. Means are for detected traces only and mean P_r does not include values >100%. Since the P_r for S5_120911 exceeds 100% this may indicate that the spikes on the tail of the main peak (Fig. 7b) are erroneous.

Name	Date	Time	V_i	Trace?	u	D	b	Q_p	A_c	P_r	Q_s	Q_s	u_s	u_s	A_m
			(ml)		(m s ⁻¹)	(m ² s ⁻¹)	(m)	(m ³ s ⁻¹)	(ppb minute ⁻¹)	(%)	(m ³ s ⁻¹)	type	(m s ⁻¹)	type	(m ²)
S7	05 Jun /06/ 2011	<u>19:02:00</u>	160	Y	0.073	2.907*	11.51*	2.14	70.1	23.5					
S5	06 Jun /06/ 2011	<u>15:43:30</u>	120	Y	0.070	14.70*	178.58*	2.08	83.9	36.6	0.027	D	0.24	D	14.68
S15	08 Jun /06/ 2011	<u>17:28:30</u>	280	N							0.027	D	0.44	D	
S14	09 Jun /06/ 2011	<u>15:57:00</u>	280	N							0.535	V	1.14	V	
S12	10 Jun /06/ 2011	<u>16:22:00</u>	280	Y	0.510	0.700	0.02	2.09	466.8	87.4	0.025	Ad D	0.44	Ad D	2.06
S7	11 Jun /06/ 2011	<u>16:31:00</u>	240	Y	0.124	2.070	3.88	2.01	124.0	26.1	0.011	Ad	0.1	Ad	8.14

		<u>0</u>										D	7	D	
S5	12 Jun /06/ 2011	<u>15:35:0</u>	200	Y	0.070	9.380*	113.82	2.21	109.8	30.5	0.032	D	0.2	D	15.8
		<u>0</u>					*						5	D	8
S15	13 Jun /06/ 2011	<u>13:17:3</u>	200	Y	0.283	71.400	144.08	3.00	123.1	46.3	0.013	D	0.2	D	5.36
		<u>0</u>											7		
S14	14 Jun /06/ 2011	<u>13:01:0</u>	200	Y	0.583	1.300	0.06	2.35	284.5	83.9	0.438	V	1.2	V	2.39
		<u>0</u>											4		
S3	15 Jun /06/ 2011	<u>10:36:0</u>	80	Y**											
		<u>0</u>													
S5	27 Jul /07/ 2011	<u>13:00:4</u>	200	Y	0.229	1.980	9.91	1.98	207.5	51.6	0.031	D	0.1	D	4.38
		<u>0</u>											3		
S15	28 Jul /07/ 2011	<u>15:28:3</u>	240	Y	0.439	1.570	0.22	2.85	196.4	58.6	0.010	D	0.2	D	3.25
		<u>0</u>											7		
S14	29 Jul /07/ 2011	<u>15:12:0</u>	160	Y	0.470	2.600	0.83	1.87	74.7	21.9	0.874	V	2.1	V	2.92
		<u>0</u>									†		3		
S12	30 Jul /07/ 2011	<u>14:45:4</u>	160	Y	0.487	9.300	5.23	2.16	68.6	23.2	0.341	D	0.4	D	2.56
		<u>0</u>											3		
S7	31 Jul /07/ 2011	<u>13:13:3</u>	200	N							0.028	D	0.2	D	
		<u>0</u>											4		
S14	01 Aug /08/ 2011	<u>12:07:3</u>	120	Y	0.731	1.240	0.26	4.47	41.0	38.3	0.888	V	2.1	V	3.66
		<u>0</u>									†		6		

S15	01 Aug /08/2011	14:43:0 0	120	Y	0.576	1.230	0.35	4.47	42.9	40.1	0.014	D	0.3 0	D	3.89
S12	02 Aug /08/2011	14:45:3 0	160	Y	0.699	1.440	0.22	4.47	69.7	48.8	0.147	Ad D	0.5 0	D	3.30
S7	03 Aug /08/2011	13:50:0 0	190	N							0.032	D	0.2 8	D	
S5	04 Aug /08/2011	11:19:3 5	195	N							0.028	D	0.1 4	D	
S5	12 Sep /09/2011	17:10:0 0	200	Y	0.063	0.09*	1.16*	7.22	179.9	163. 0					
S15	13 Sep /09/2011	13:28:3 0	240	Y	0.578	4.50	0.47	5.16	134.6	72.6	0.022	D	0.5 0	D	4.43
S14	14 Sep /09/2011	12:26:0 0	120	Y	0.697	1.40	0.27	6.02	45.0	56.6	0.378 †	V	0.9 2	V	4.60
S12	14 Sep /09/2011	15:15:0 0	160	Y	0.593	3.54	1.16	6.34	71.4	71.0	0.196	D	0.4 9	D	5.54
S7	15 Sep /09/2011	14:19:0 0	200	Y***							0.006	D	0.2 5	D	
Mean (all)					0.404	7.30	26.22	3.49	133.0	48.0	0.203		0.6 3		5.44
Mean (upper)					0.554	8.35	12.76	3.77	134.9	54.1	0.279		0.8		3.66

								0	
Mean (lower)	0.105	5.19	53.14	2.94	129.2	33.6	0.022	0.2	10.7
								1	7

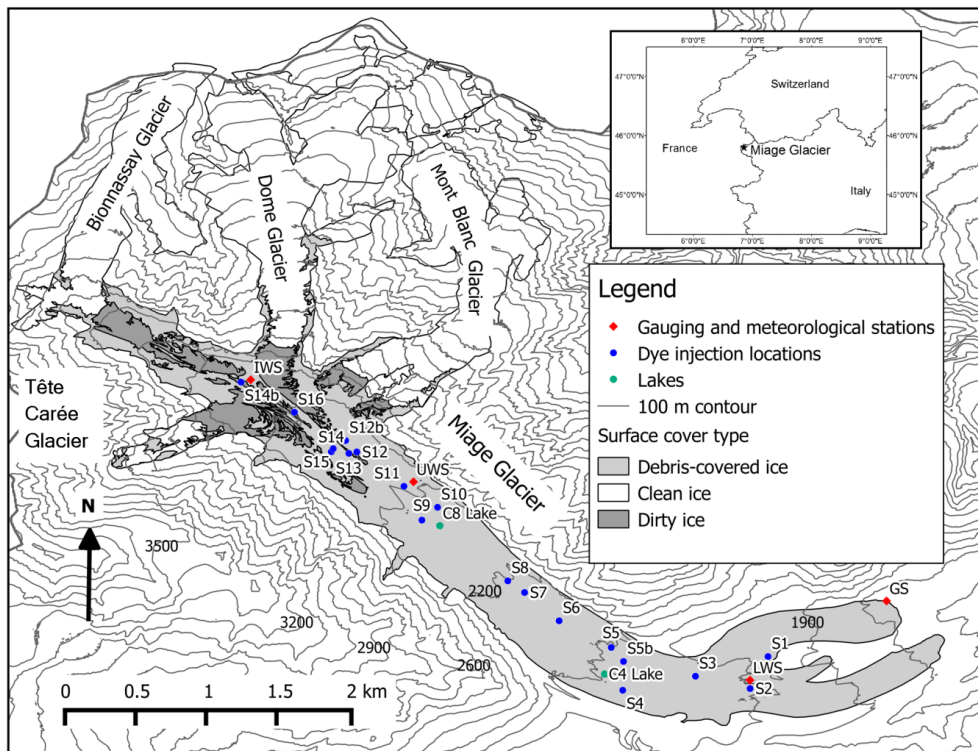


Figure 1 Map of Miage Glacier showing location of monitoring stations, lakes and dye tracing points. Inset shows location of Miage Glacier in the Alps. 'IWS' is the ice weather station, 'UWS' the upper weather station, 'LWS' the lower weather station and 'GS' the gauging station.

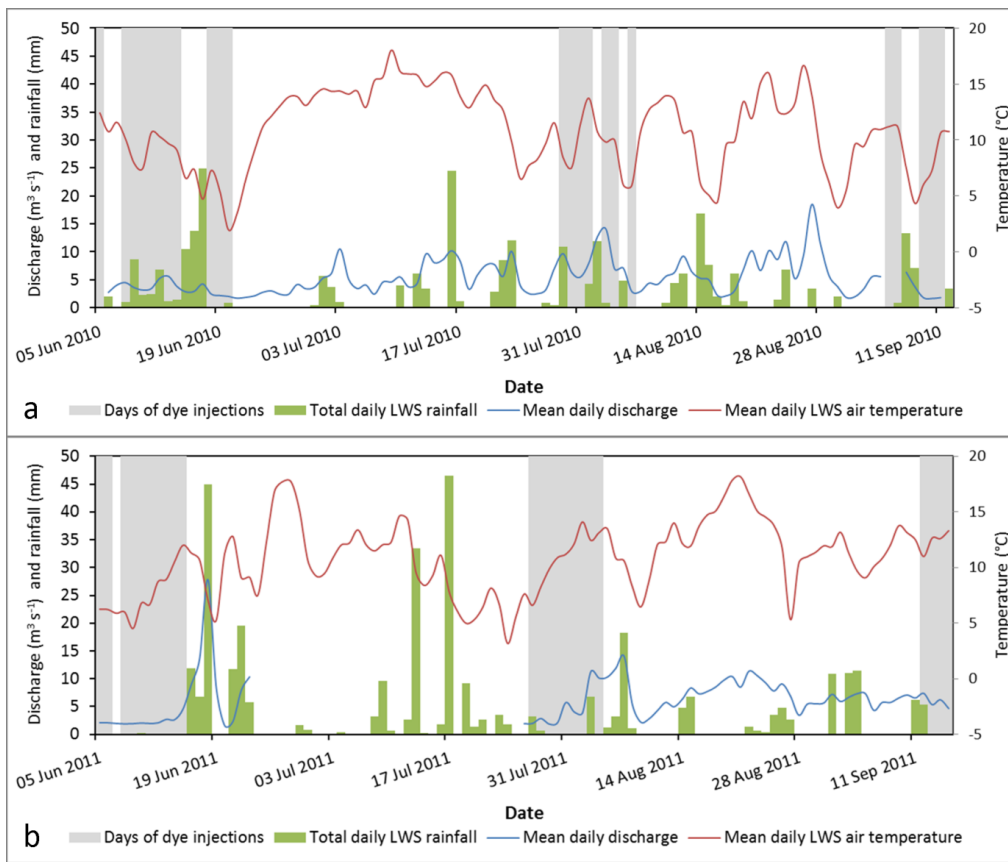


Figure 2 Meteorological conditions and **proglacial** discharge during the a) 2010 and b) 2011 field seasons. Grey bars indicate days when dye injections were conducted.



Figure 3 a) the englacial conduit above the S8 stream, b) dye tracing the S12 stream in September 2011 and c) dye tracing S14 in July 2011.

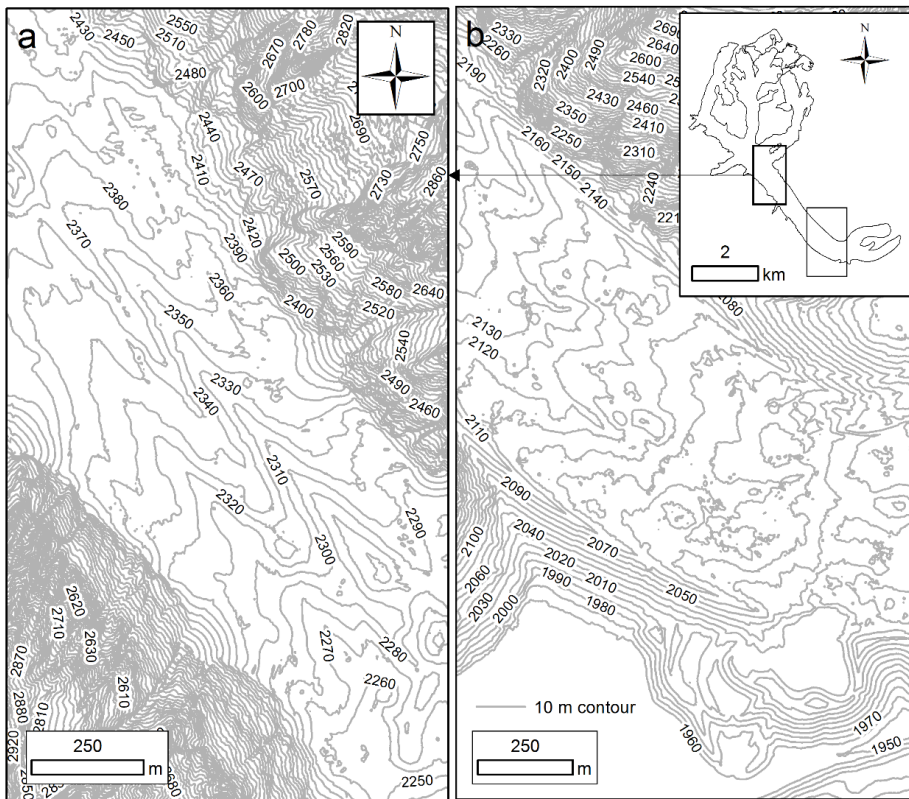


Figure 4 Topographic influence on supraglacial hydrology. **Panel a)** The left inset shows the clear along-glacier ridge and valley topography associated with the central, eastern and western moraines on the upper tongue, with panel b). The right inset showing the hummocky topography on the lower glacier. Both panels insets show contours at 10 m intervals. Source: Regione Autonoma Valle d'Aosta DEM.

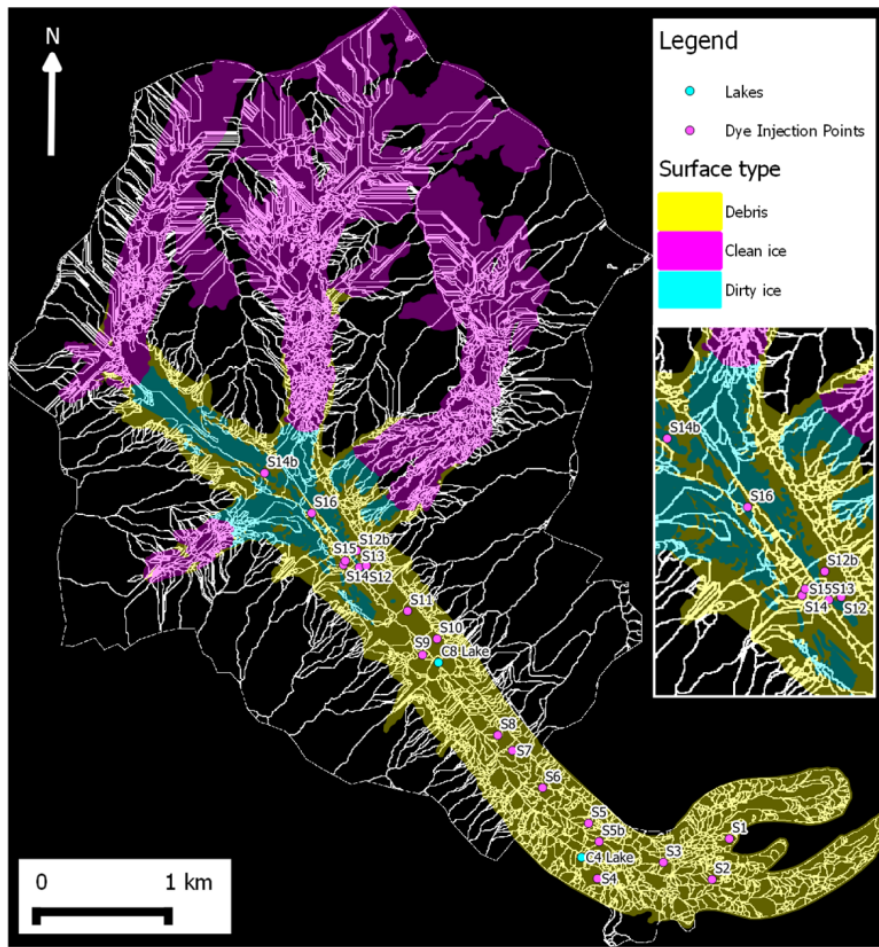


Figure 5 A map of the outlines (shown as white lines) of the modelled supraglacial catchments. Inset shows the central ablation area, upstream of the cluster of moulines near the upper limit of the continuous debris cover.

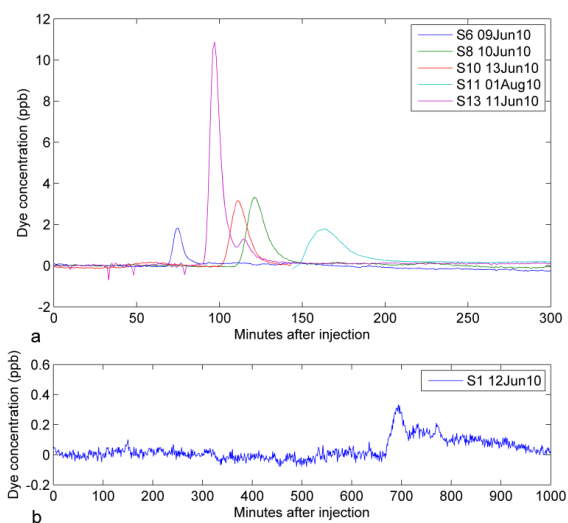


Figure 6 Dye return curves from streams that were only traced once (injections conducted in 2010). Note that vertical and horizontal scales differ between subplots.

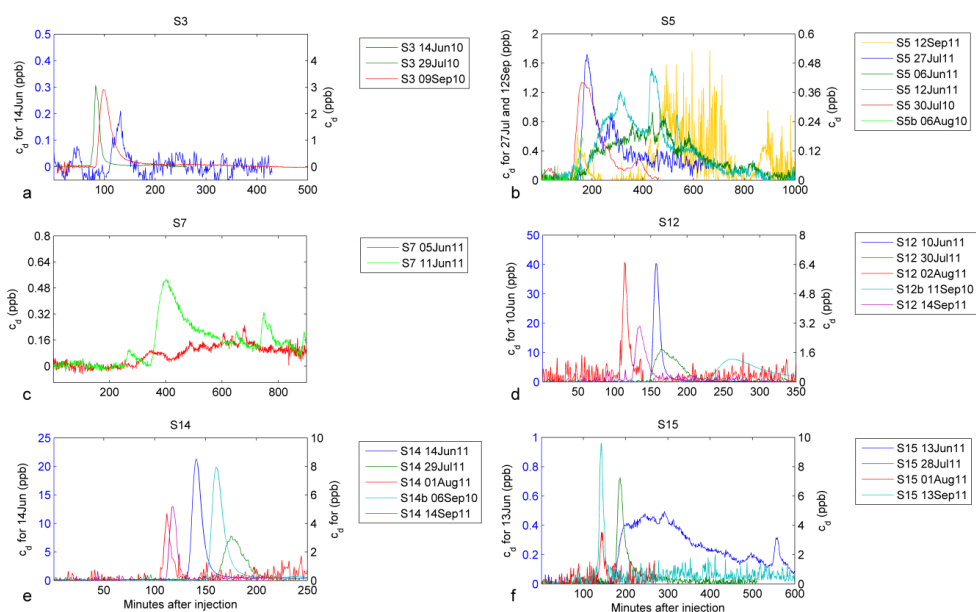


Figure 7 Repeat dye return curves from single injection points (including injections performed in both 2010 and 2011), where c_d is the dye concentration. The injection points S3, S5 and S7 (a, b and c) are on the lower glacier, while injection points S12, S14 and S15 (d, e and f) are on the upper glacier. Note that vertical and horizontal scales differ.

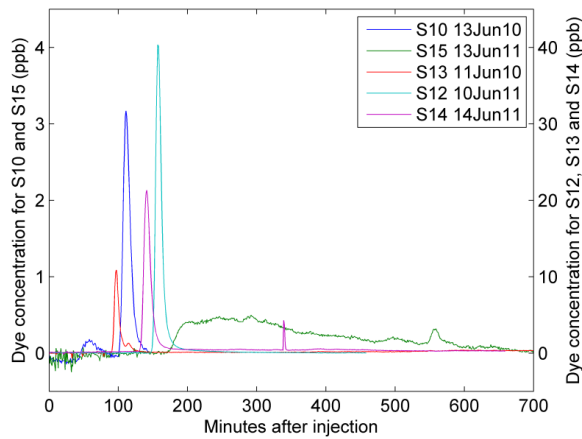


Figure 8 Dye return curves from the upper glacier streams injected in June of both 2010 and 2011. Note that vertical scales differ.

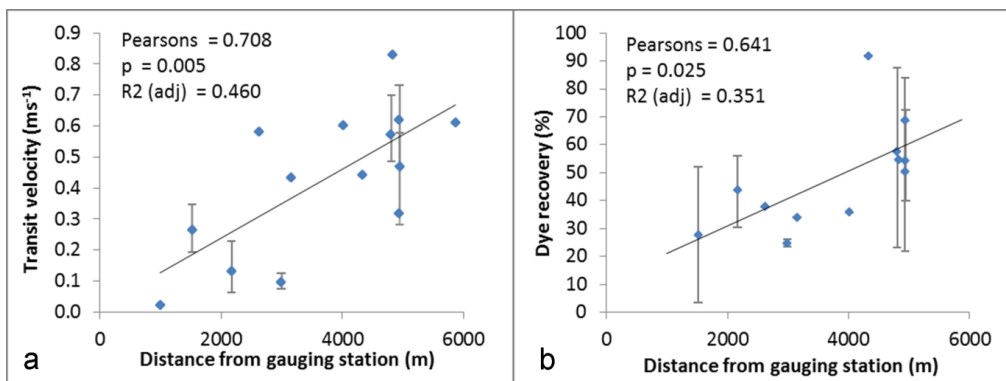


Figure 9 Relationship between the distance to gauging station and a) average injection point u , and b) average injection point P_r , including all 2010 and 2011 data. P_r in b) does not include values over 100%. Bars show the range of values measured for streams where multiple injections were conducted.

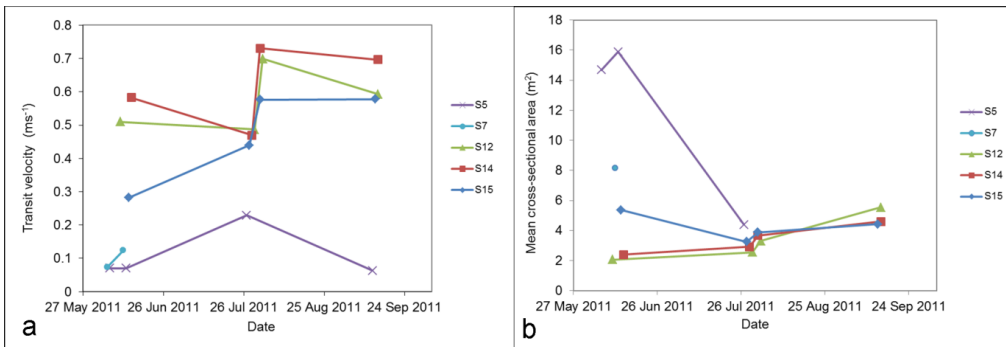


Figure 10 a) Dye trace u variations over the 2011 season, and b) mean A_m variations over the 2011 season.